Chinese Journal of Structural Chemistry

COMMUNICATION

Sulfonate-Functionalized Polyoxovanadate-Based Metal-Organic Polyhedra for Enhanced Proton Conduction *via* the Synergy of Linker and Metal Cluster Vertex

Yu Zhang[1†], Shan-Shan Liu[1†], Bo Li[2†], Hanqi You[1], Longxi Zhang[1], Zhenyi Zhang[3], Hong-Ying Zang[2*], Qi Zheng[4*] and Weimin Xuan[1*]

[1]*College of Chemistry, Chemical Engineering and Biotechnology & State Key Laboratory for Modification of Chemical Fibers and Polymer Materials, Donghua University, Shanghai 201620, China*

[2]*Key Laboratory of Polyoxometalate and Reticular Material Chemistry of Ministry of Education at Universities of Jilin Province, Faculty of Chemistry, Northeast Normal University, Changchun 130024, China*

[3]*Bruker (Beijing) Scientific Technology Co., Ltd 9F, Building No.1, Lane 2570, Hechuan Rd, Minhang District, Shanghai 200233, China*

[4]*State Key Laboratory for Modification of Chemical Fibers and Polymer Materials, College of Materials Science and Engineering, Donghua University, Shanghai 201620, China*

ABSTRACT Metal-organic polyhedra (MOPs) have emerged as novel porous platforms for proton conduction, however, the concerted employment of both linker and metal cluster vertex is rarely applied for the fabrication of MOPs-based high conducting materials. Herein we report the synthesis of sulfonate-functionalized polyoxovanadate-based MOPs for enhanced proton conduction *via* the synergistic effect from linker and metal cluster node. MOPs **1** and **2** exhibit octahedral cage configuration constructed from $\{V_5O_9Cl\}$ vertex and 5-sulfoisophthalate linker. Owing to the ordered packing of octahedral cages along three axes, 3D interpenetrated open channels that are lined with high-density sulfonates are thus formed within **2**. Coupled with the proton-conductive $\{V_5O_9Cl\}$ vertexs as well as protonated counterions, an extensive H-bonded network is therefore generated for facile proton transfer. **2** exhibits high proton conductivity of 3.02×10^{-2} S cm^{-1} at 65 °C under 90% RH, recording the highest value for MOPs pellet sample. This value is enhanced ~1 order of magnitude compared with that of carboxylate-functionalized analogue **3**, clearly illustrating the advantage of combining linker and metal cluster node for enhanced proton conduction. This work will further promote the exploitation of high proton conductive MOPs-based materials by the synergy design strategy.

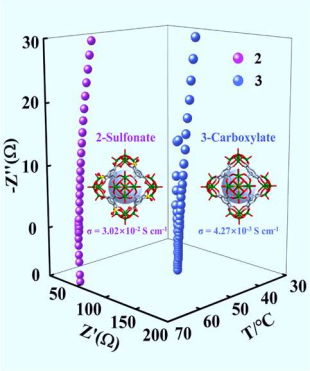

Keywords: metal-organic polyhedra, proton conduction, polyoxovanadate, synergistic effect

INTRODUNTION

Consumption of conventional fossil fuels to produce energy has caused serious energy crisis and environmental pollution to the world.[1] In the context of searching for renewable energy conversion technology, fuel cells provide a green alternative to transform chemical energy into electricity.[2] Particularly, proton exchange membrane fuel cells (PEMFCs) have been regarded as one type of very promising fuel cells for power supply in both power stations and portable electronic devices.[3] As the key component of PEMFCs, proton exchange membrane (PEM) should meet the requirements of high proton conductivity, excellent stability and durability as well as competitive low-cost.[4-6] Although the commercially available Nafion films are predominantly used in PEMFCs, their high cost and low operating temperature (< 80 °C) limit the wide application. As such, a variety of crystalline porous materials including metal-organic frameworks (MOFs),[7-13] zeolites[14] and covalent organic frameworks (COFs)[15-17] have been developed as promising solid-state proton conductors owing to the presence of intrinsic channels which favor the proton transfer and facile installation of proton conducting functionality.[18] Some prominent representatives can not only be prepared from cheap and simple starting materials but also show superior proton conductivity under harsh conditions and over wide operation temperature.

Inspired by the progress achieved by the infinite porous materials mentioned above, metal-organic polyhedra (MOPs),[19-25] a class of discrete porous molecular containers, have been recently utilized as porous platforms for proton conduction.[26-30] The general strategy is to make the use of intrinsic porosity within the cage as well as the intermolecular channels as the proton-hopping pathway while incorporating proton transferring sites such as carboxylic acid, sulfonic acid and guest water either on the organic linkers or into the porosity.[31,32] The carboxylate and sulfonate functionalized MOPs have exhibited high proton conductivity compared with that of Nafion films.[26,29] Despite the significant advance, the development of MOP-based proton conductors is still limited, and to the best of our knowledge, the employment of both linker and metal/cluster node as proton conducting sites is hardly explored for such materials.[28]

Polyoxometalates (POMs) are a unique class of discrete anionic metal-oxo clusters with O-enriched surfaces that can provide abundant proton conducting sites for efficient proton transfer.[33-36] Nevertheless, POMs suffer from the drawback of intrinsically high solubility in water, which greatly restricts their applications in fuel cells. To solve this obstacle, loading of POMs in highly porous carriers such as MOFs and COFs has been proved to be an effi-

DOI: 10.14102/j.cnki.0254-5861.2022-0127

cient approach to construct stable POM-based proton conductors.[37,38] In contrast, anchoring POMs into porous MOPs for proton conduction has been rarely explored although POMs are wildly used as metal cluster vertexes to fabricate MOPs.[39-46] In fact, if the linkers, guest molecules and even the counter ions are favorable for proton conduction, the POM-derived MOPs can not only make use of POM cluster vertexes but also all the other components to facilitate the formation of hydrogen bond networks. This provides a feasible approach to construct MOP-based high-performance proton conductors *via* synergistic effect.

Bearing this in mind, herein we report the synthesis of two octahedral MOPs $(NMe_4)_x(NHMe_3)_{14-x}[Na_6(V_5O_9Cl)_4(L)_8Cl_4(C_2H_4N_4)_4]\cdot$(**1**), $(NH_2Me_2)_{12}[(V_5O_9Cl)_6(L)_8]\cdot 11CH_3OH\cdot 12DMF$ (**2**) and $(NH_2Me_2)_{12}[(V_5O_9Cl)_6(C_9H_3O_6)_8]$ (**3**), using the in-situ formed polyoxovanadate $\{V_5O_9Cl\}$ as vertex and 5-sulfoisophthalate (L) as linker (Scheme 1). Owing to the coexistence of sulfonates and POM clusters in the skeleton, coupled with protonated dimethylamine as proton conductors, compound **2** shows high proton conductivity of 3.02×10^{-2} S cm^{-1} at 65 °C and 90% RH, which is the highest value reported for MOPs pellet samples. In contrast, the octahedral MOP **3** constructed from the same cluster and trimesic acid exhibits much lower proton conductivity of 4.27×10^{-3} S cm^{-1} under the same conditions, indicating the unique advantage of incorporating both proton-conductive metal cluster vertex and sulfonate on the linker for the enhancement of proton conductivity *via* synergistic effect.

RESULTS AND DISCUSSION

Syntheses and Structures of 1 and 2. The crystal of compound **1** was obtained under solvothermal conditions by heating a mixture of VCl_3, 5-sulfoisophthalic acid monosodium salt and 4-amino-1,2,4-triazole in DMF/CH_3OH mixture (DMF = N,N'-dimethylformamide) at 130 °C for 3 days. Single-crystal X-ray structural analysis reveals that **1** crystallizes in the monoclinic space group *C*2/*c* (Table S1). The molecular structure of **1** adopts an open octahedral cage with two vertexes missing in apical positions (Scheme 1a). The vertex consists of bowl-shaped $\{V_5O_9Cl\}$ cluster defined by one $\{VO_5\}$ tetragonal pyramid that is surrounded by four $\{VO_5Cl\}$ octahedra. The V-O bond distances in $\{V_5O_9Cl\}$ range from 1.592(5) to 2.021(4) Å (Table S2). Bond valence sum (BVS) calculations indicate that the apical vanadium is +5 and four basal plane vanadium atoms are +4, which is consistent with previous reports (Table S4).[47] Two sets of four L locate above and below the equatorial plane, respectively, with the two carboxylates connecting two adjacent $\{V_5O_9Cl\}$ vertexes while the sulfonate coordinating to the sodium counterions. There are there crystallographically independent sodium atoms. The octahedral coordination sphere of Na1 is fulfilled by five oxygen atoms from sulfonates and one chloride, while Na2 adopts distorted mono-capped triangular prism coordination geometry defined by six oxygen atoms from three sulfonates and one chloride as the cap. The coordination environment of Na3 can also be described as mono-capped triangular prism surrounded by three sulfonates and two 4-amino-1,2,4-triazole molecules which are encapsulated within the cavity of octahedron (Figure S1). In this way, the neighbouring open cages are thus joined by two sets of $\{Na_3\}$ clusters to form a 1D zigzag chain. The void constructed from the packing of zigzag chains is occupied by protonated trimethylamine and tetramethyl ammonium which are probably derived from the decomposition of 4-amino-1,2,4-triazole (Figure S2).

It should be noted that 4-amino-1,2,4-triazole is indispensable for the synthesis of **1**. This compound on one hand can behave as ligand coordinating to sodium atoms together with sulfonates on 5-sulfoisophthalate; this prevents the further coordination of sulfonates to the V centers in $\{V_5O_9Cl\}$ and thus allows the formation of open octahedral cage. On the other hand, the counter cations (trimethylammonium and tetramethyl ammonium) derived from 4-amino-1,2,4-triazole also play important roles in directing the self-assembly. Owing to the bigger size as compared with dimethylammonium, trimethylammonium and tetramethyl ammonium will accelerate the growth and precipitation of crystals. This can reduce the possibility of sulfonates to interact with V centers in $\{V_5O_9Cl\}$, therefore leaving sulfonates uncoordinated, which in turn facilitates the formation of open cage-like **1** instead of a closed octahedron.

Using $Li_2B_4O_7$ instead of 4-amino-1,2,4-triazole afforded com-

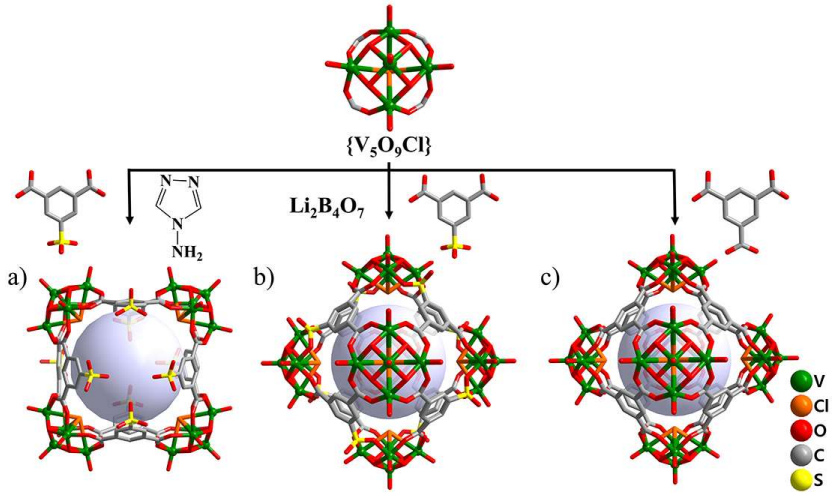

Scheme 1. Schematic representation of the preparation of **1** a), **2** b), and **3** c). Hydrogen atoms are omitted for clarity. Large light purple spheres represent the free space inside the cages.

Chin. J. Struct. Chem. **2022**, 41, 2208012-2208017
DOI: 10.14102/j.cnki.0254-5861.2022-0127

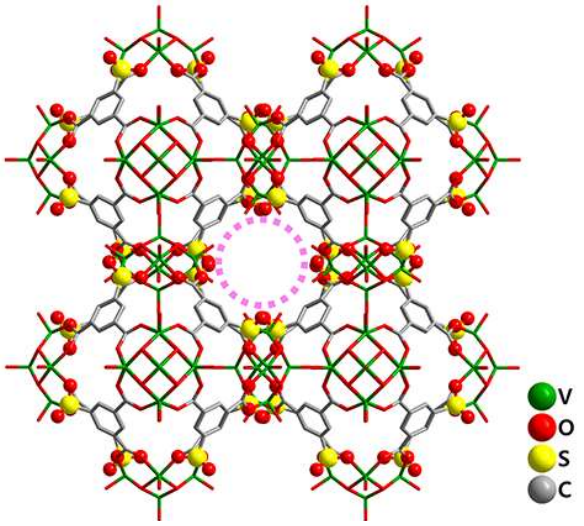

Figure 1. The view of the open channels lined with sulfonates in **2**. The channel is highlighted by pink dotted circle.

pound **2**. Borates are well known for their critical roles in guiding the self-assembly of polyoxovanadates.[48,49] The presence of $Li_2B_4O_7$ during the synthesis is supposed to facilitate and stabilize the formation of $\{V_5O_9Cl\}$ build blocks, which is then gradually substituted by 5-sulfoisophthalate to induce the formation of octahedron **2**. Similar phenomenon has been observed during the assembly of gigantic polyoxoniobates $\{Nb_{288}\}$ and $\{Nb_{114}\}$ wherein $Li_2B_4O_7$ is essential for the generation of such clusters.[50,51] Single crystal X-ray structural analysis shows that **2** crystallizes in the cubic space group *Fm*$\bar{3}$ (Table S1). As depicted in Scheme 1b, the molecular structure of **2** features a regular octahedral cage similar to reported **3** (Scheme 1c) in which the octahedron is built from 1,3,5-benzenetricarboxylate and $\{V_5O_9Cl\}$.[52] In contrast to **1**, both the carboxylates and sulfonates in **2** coordinate to V centers in $\{V_5O_9Cl\}$, thus generating a closed octahedron. The V-O bond distances and the valence of V in $\{V_5O_9Cl\}$ are almost the same as **1** (Table S3 and S5). Bond valence sum (BVS) calculations show the same result as **1**, which is further confirmed by XPS with the ratio of V^{IV} to V^{V} as 4:1 (Figure S3). Owing to the high symmetry, the ordered packing of **2** gives rise to interpenetrated channels along three axes with a size of ~5.0 × 5.0 Å (Figure 1 and Figure S4). More importantly, sulfonates are evenly lined on the inner surface of the open channels with high-density, providing a 3D pathway for proton transfer (Figure 1). According to PLATON analysis,[53] the estimated solvent-accessible volume for **2** is 13859.7 Å^3 (53%), which is accommodated by dimethylammonium cations and guest molecules of DMF and MeOH.

Due to the poor repeatability of **1**, only **2** was subjected to basic characterization and used for further property study. The phase purity of **2** could be proved by the good agreement between experimental and simulated PXRD pattern (Figure S6). TGA analysis indicated the weight loss (17.31%) between 50 and 340 °C is due to the removal of 11 CH_3OH and 12 DMF, followed by a weight loss (8.63%) corresponding to the release of 12 $[NH_2Me_2]^+$ cations from 340 to 380 °C. Subsequently, the skeleton is decomposed at higher temperature (Figure S7). The characteristic peaks of -NH_2 group on $[NH_2Me_2]^+$ (3435 cm^{-1}), V=O (1007 and 986 cm^{-1}) and V-O-V (529-772 cm^{-1}) as well as sulfonates stretching vibration (1201 and 1048 cm^{-1}) can be clearly identified from IR spectrum, further confirming the composition and structural integrity of **2** (Figure S8).[52,54]

Proton Conduction of 2 and 3. Compound **2** contains high-density hydrophilic sites, such as sulfonates on the linkers, terminal oxygen atoms on $\{V_5O_9Cl\}$ vertexes, and protonated counterions (e.g. $[NH_2Me_2]^+$), implying the potential of this material to act as a good solid proton conductor. Therefore, the proton conductivity of crystalline powder sample **2** was measured by alternating current (AC) impedance measurement under various relative humilities (RH 60%-90%) and temperatures (30-65 °C). At 30 °C, the proton conductivity of **2** is 1.29×10^{-7} and 5.43×10^{-3} S cm^{-1} when the RH is 60% and 90%, respectively (Table S6). The proton conductivity increases 4 orders of magnitude with RH enhancing from moderate to high humidity and the proton conductivity rises linearly with the increase of RH (Figure S9), suggesting that water molecules play a momentous role in proton conducting and migration within the 3D channels of **2**. As demonstrated by the water-vapor adsorption and desorption isotherms (Figure S10), **2** exhibits an excellent water-adsorption capacity (318 mg/g) especially at higher RH. This allows the formation of more hydrogen-bonds *via* adsorbed water molecules, thereby further facilitating the proton transport.

To further exploit the relationship between temperature and proton conductivity, the temperature-dependent proton conducting performance of **2** was measured from 30 to 65 °C at 90% RH (Figure 2a). As shown in Figure 3a, the proton conductivity of **2** enhances linearly with the increase of temperature, because higher temperature will facilitate the formation of H_3O^+ and hasten the proton migration.[55] Even at 30 °C, relatively high conductivity of 5.43×10^{-3} S cm^{-1} can be obtained (Table S8), indicating the extensive hydrogen-bonded network formed by sulfonate group, $\{V_5O_9Cl\}$ vertex, $[NH_2Me_2]^+$ and free water molecules in the 3D

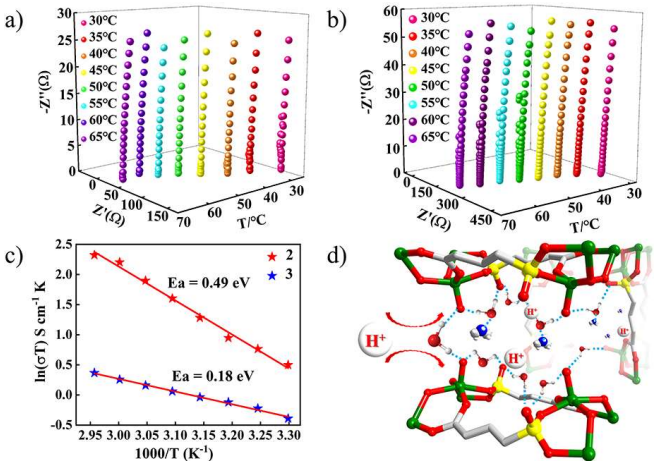

Figure 2. a) Nyquist plots of compound **2** at 90% RH from 30 to 65 °C. b) Nyquist plots of compound **3** at 90% RH from 30 to 65 °C. c) Arrhenius plots with activation energies (E_a) for **2** and **3** at 90% RH. d) The proposed mechanism of proton conduction of **2**.

DOI: 10.14102/j.cnki.0254-5861.2022-0127

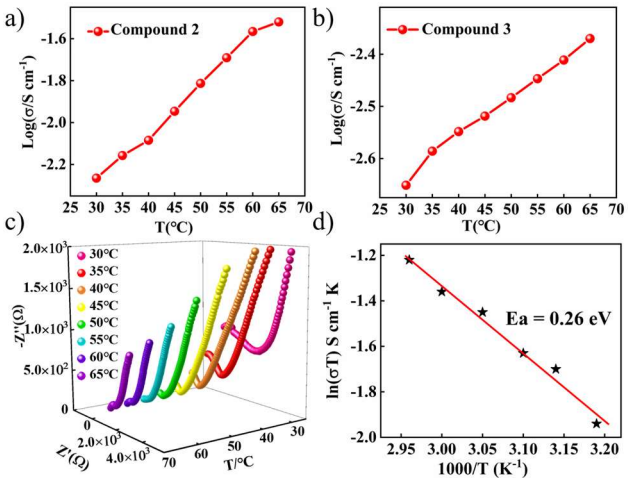

Figure 3. a) Proton conductivity of compound **2** at different temperatures. b) Proton conductivity of compound **3** at different temperatures. c) Nyquist plots of compound **2** at 80% RH from 30 to 65 °C. d) Arrhenius plots with activation energies (E_a) for **2** at 80% RH.

channels can efficiently promote the proton transfer even at low temperature.[31,56] When above 65 °C, the proton conductivity of **2** reaches 3.02×10^{-2} S cm^{-1}, which is comparable to that of commercial Nafion, and ranks among the highest proton conducting performance recorded by high-proton conductors, such as MOFs and COFs.[26,57,58] Furthermore, this value is also comparable with that of the best POM-based proton conductors (Table S11).[59-61] More importantly, this value represents the highest proton conductivity reported so far by MOPs in compressed pellet and is only slightly inferior to the benchmark 5.8×10^{-2} S cm^{-1} achieved by the single crystal sample of MOP $[Cr_4In_4(Himdc)_{12}]$ (Table S10).[25]

In order to elucidate the effect of sulfonates on the proton conduction, **3** was prepared and used for proton conductivity measurement under identical conditions. **3** is isostructural analogue of **2**, composed of octahedral cage built from $\{V_5O_9Cl\}$ and trimesic acid (Scheme 1c and Figure S5).[52] The proton conductivity of **3** only increase ~2 times from 2.23×10^{-3} to 4.27×10^{-3} S cm^{-1} when the temperature varies from 30 to 65 °C (Figure 2b and 3b and Table S9). In contrast, in the presence of sulfonate, the conductivity of **2** enlarges almost 6 times and the highest value obtained at 65 °C is around one order of magnitude higher than that of **3** (Figure 3a). Since the crystal structure and packing mode are quite similar to each other, the dramatic difference in proton conductivity for **2** and **3** mainly derives from the dense alignment of sulfonate within the 3D open channels of **2**, resulting in more pathways and sites for proton mobility.

To probe the mechanisms of proton conduction for **2** and **3**, the activation energy (E_a) was measured at 90% RH in the range of 30-65 °C. The E_a of **3** is 0.18 eV based on the calculation of Arrhenius plot (Figure 2c), implying that the protons migrate by Grotthuss mechanism (E_a < 0.4 eV).[62] The E_a of **2** is estimated as 0.49 eV, a value falling between the standard of Grotthuss mechanism and vehicle mechanism (E_a > 0.5 eV) (Figure 2c). We therefore propose that the protons transfer mainly through the Grotthuss mechanism, and partially by vehicle mechanism.[63-65] This is also supported by the E_a (0.26 eV) measured at 80% RH (Table S7, Figure 3c and 3d), which further confirms the predominate role of Grotthuss mechanism. Based on what discussed above, the proton transfer pathway for **2** is depicted (Figure 2d). In addition to the extended H-bonded proton-hopping pathways constructed from $-SO_3^-$, $\{V_5O_9Cl\}$ metal cluster, the absorbed water molecules and $[NH_2Me_2]^+$, the H_3O^+ can also serve as proton carrier to deliver the protons *via* self-diffusion based on vehicular mechanism. Moreover, **2** and **3** show outstanding integrity after AC impedance measurement test (Figure S11 and S12).

CONCLUSION

In conclusion, we have showed a strategy that combines the proton conducting POM cluster vertex and linker to build two sulfonate-functionalized polyoxovanadate-based MOPs for enhanced proton conductivity. Due to the synergistic effect from $\{V_5O_9Cl\}$ vertexes and sulfonates on linkers, extensive hydrogen bonded network is formed together with the protonated counterions as well as the adsorbed water molecules. As such, **2** exhibits high proton conductivity of 3.02×10^{-2} S cm^{-1} at 65 °C under 90% RH, which records the highest value for MOPs measured in the pellet sample. In particular, this value is about 1 order of magnitude higher than that of carboxylate-functionalized analogue **3**, demonstrating the significance of installing proton conducting sites on both metal cluster vertex and linker. This work not only sheds lights on developing high proton-conductive MOP materials using the synergy of linker and vertex, but also may provide a general strategy to improve the proton conductivity for coordination-driven materials.

ACKNOWLEDGEMENTS

This work was supported by the National Natural Science Foundation of China (Nos. 92161111, 21901037, 21901038, 21871042), Shanghai Pujiang Program (No. 19PJ1400200), and the Program for Professor of Special Appointment (Eastern Scholar) at Shanghai Institutions of Higher Learning and International Cooperation Fund of Science and Technology Commission of Shanghai Municipality (No. 21130750100). We also thank the staff from BL17B beamline of National Facility for Protein Science in Shanghai (NFPS) at Shanghai Synchrotron Rdiation Facility, for assistance during data collection.

AUTHOR CONTRIBUTION

Yu Zhang, Shan-shan Liu and Bo Li contribute equally to this work.

AUTHOR INFORMATION

Corresponding authors. Emails: weiminxuan@dhu.edu.cn, qi.zheng@dhu.edu.cn and zanghy100@nenu.edu.cn

COMPETING INTERESTS

The authors declare no competing interests.

ADDITIONAL INFORMATION

Supplementary information is available for this paper at http://manu30.magtech.com.cn/jghx/EN/10.14102/j.cnki.0254-5861.2022-0127

DOI: 10.14102/j.cnki.0254-5861.2022-0127

For submission: https://mc03.manuscriptcentral.com/cjsc

REFERENCES

(1) Chu, S.; Majumdar, A. Opportunities and challenges for a sustainable energy future. *Nature* **2012**, 488, 294-303.

(2) Wang, S. Y.; Jiang, S. P. Prospects of fuel cell technologies. *Natl. Sci. Rev.* **2017**, 4, 161-163.

(3) Guo, Z. M.; Perez-Page, M.; Chen, J. N.; Ji, Z. Q.; Holmes, S. M. Recent advances in phosphoric acid-based membranes for high-temperature proton exchange membrane fuel cells. *J. Energy Chem.* **2021**, 63, 393-429.

(4) Zhang, H. W.; Shen, P. K. Recent development of polymer electrolyte membranes for fuel cells. *Chem. Rev.* **2012**, 112, 2780-2832.

(5) Jiao, K.; Xuan, J.; Du, Q.; Bao, Z. M.; Xie, B.; Wang, B. W.; Zhao, Y.; Fan, L. H.; Wang, H. Z.; Hou, Z. J.; Huo, S.; Brandon, N. P.; Yin, Y.; Guiver, M. D. Designing the next generation of proton-exchange membrane fuel cells. *Nature* **2021**, 595, 361-369.

(6) Chen, J. N.; Bailey, J. J.; Britnell, L.; Perez-Page, M.; Sahoo, M.; Zhang, Z.; Strudwick, A.; Hack, J.; Guo, Z. M.; Ji, Z. Q.; Martin, P.; Brett, D. J. L.; Shearing, P. R.; Holmes, S. M. The performance and durability of high-temperature proton exchange membrane fuel cells enhanced by single-layer graphene. *Nano Energy* **2022**, 93, 106829.

(7) Lim, D. W.; Kitagawa, H. Proton transport in metal-organic frameworks. *Chem. Rev.* **2020**, 120, 8416-8467.

(8) Liu, R. l.; Wang, D. Y.; Shi, J. R.; Li, G. Proton conductive metal sulfonate frameworks. *Coord. Chem. Rev.* **2021**, 431, 213747.

(9) Xie, X. X.; Yang, Y. C.; Dou, B. H.; Li, Z. F.; Li, G. Proton conductive carboxylate-based metal-organic frameworks. *Coord. Chem. Rev.* **2020**, 403, 213100.

(10) Wahiduzzaman, M.; Wang, S. J.; Schnee, J.; Vimont, A.; Ortiz, V.; Yot, P. G.; Retoux, R.; Daturi, M.; Lee, J. S.; Chang, J. S.; Serre, C.; Maurin, G.; Devautour-Vinot, S. A high proton conductive hydrogen-sulfate decorated titanium carboxylate metal-organic framework. *ACS Sustain. Chem. Eng.* **2019**, 7, 5776-5783.

(11) Xue, W. L.; Deng, W. H.; Chen, H.; Liu, R. H.; Taylor, J. M.; Li, Y. K.; Wang, L.; Deng, Y. H.; Li, W. H.; Wen, Y. Y.; Wang, G. E.; Wan, C. Q.; Xu, G. MOF-directed synthesis of crystalline ionic liquids with enhanced proton conduction. *Angew. Chem. Int. Ed.* **2021**, 60, 1290-1297.

(12) Lin, Y.; Li, W. H.; Wen, Y. Y.; Wang, G. E.; Ye, X. L.; Xu, G. Layer-by-layer growth of preferred-oriented MOF thin film on nanowire array for high-performance chemiresistive sensing. *Angew. Chem. Int. Ed.* **2021**, 60, 25758-25761.

(13) Guo, S. S.; Huang, L. L.; Ye, Y. X.; Liu, L. Z.; Yao, Z. Z.; Xiang, S. C.; Zhang, J. D.; Zhang, Z. J. Carbazole based anionic MOF for proton conductivity. *Chin. J. Struct. Chem.* **2021**, 40, 55-60.

(14) Hana, W.; Kwana, S. M.; Yeung, K. L. Zeolite applications in fuel cells: water management and proton conductivity. *Chem. Eng. J.* **2012**, 187, 367-371.

(15) Xu, H.; Tao, S. S.; Jiang, D. L. Proton conduction in crystalline and porous covalent organic frameworks. *Nat. Mater.* **2016**, 15, 722-726.

(16) Jin, E. Q.; Geng, K. Y.; Fu, S.; Yang, S.; Kanlayakan, N.; Addicoat, M. A.; Kungwan, N.; Geurs, J.; Xu, H.; Bonn, M.; Wang, H. I.; Smet, J.; Kowalczyk, T.; Jiang, D. l. Exceptional electron conduction in two-dimensional covalent organic frameworks. *Chem* **2021**, 7, 3309-3324.

(17) Liu, L.; Yin, L. Y.; Cheng, D. M.; Zhao, S.; Zang, H. Y.; Zhang, N.; Zhu, G. S. Surface-mediated construction of an ultrathin free-standing covalent organic framework membrane for efficient proton conduction. *Angew. Chem. Int. Ed.* **2021**, 60, 14875-14880.

(18) Liu, G. M.; Ma, W. J.; Wang, Y.; Yang, Y.; Song, X. J. Computational insights into the excited state intramolecular proton transfer reactions in ortho-hydroxylated oxazolines. *Chin. J. Struct. Chem.* **2021**, 40, 540-548.

(19) Gosselin, A. J.; Rowland, C. A.; Bloch, E. D. Permanently microporous metal-organic polyhedra. *Chem. Rev.* **2020**, 120, 8987-9014.

(20) Fujita, D.; Ueda, Y.; Sato, S.; Mizuno, N.; Kumasaka, T.; Fujita, M. Self-assembly of tetravalent Goldberg polyhedra from 144 small components. *Nature* **2016**, 540, 563-566.

(21) Yamashina, M.; Tanaka, Y.; Pittelkow, M.; Nitschke, J. R.; Lavendomme, R.; Ronson, T. K. An antiaromatic-walled nanospace. *Nature* **2019**, 574, 511-515.

(22) Jiao, J. J.; Tan, C. X.; Li, Z. J.; Liu, Y.; Han, X.; Cui, Y. Design and assembly of chiral coordination cages for asymmetric sequential reactions. *J. Am. Chem. Soc.* **2018**, 140, 2251-2259.

(23) Dong, J. Q.; Liu, Y.; Cui, Y. Supramolecular chirality in metal-organic complexes. *Acc. Chem. Res.* **2021**, 54, 194-206.

(24) Wei, J. W.; Zhao, L.; He, C.; Zheng, S. J.; Reek, J. N. H.; Duan, C. Y. Metal-organic capsules with NADH mimics as switchable selectivity regulators for photocatalytic transfer hydrogenation. *J. Am. Chem. Soc.* **2019**, 141, 12707-12716.

(25) Li, Y. G.; Dong, J. Q.; Gong, W.; Tang, X. H.; Liu, Y. H.; Cui, Y.; Liu, Y. Artificial biomolecular channels: enantioselective transmembrane transport of amino acids mediated by homochiral zirconium metal-organic cages. *J. Am. Chem. Soc.* **2021**, 143, 20939-20951.

(26) Guo, T. T.; Cheng, D. M.; Yang, J.; Xu, X. X.; Ma, J. F. Calix[4]resorcinarene-based [Co_{16}] coordination cages mediated by isomorphous auxiliary ligands for enhanced proton conduction. *Chem. Commun.* **2019**, 55, 6277-6280.

(27) Samanta, D.; Mukherjee, P. S. Component selection in the self-assembly of palladium(II) nanocages and cage-to-cage transformations. *Chem. Eur. J.* **2014**, 20, 12483-12492.

(28) Saha, R.; Samanta, D.; Bhattacharyya, A. J.; Mukherjee, P. S. Stepwise construction of self-assembled heterometallic cages showing high proton conductivity. *Chem. Eur. J.* **2017**, 23, 8980-8986.

(29) Zhai, Q. G.; Mao, C. Y.; Zhao, X.; Lin, Q. P.; Bu, F.; Chen, X. T.; Bu, X. H.; Feng, P. Y. Cooperative crystallization of heterometallic indium-chromium metal-organic polyhedra and their fast proton conductivity. *Angew. Chem. Int. Ed.* **2015**, 54, 7886-7890.

(30) Xing, W. H.; Li, H. Y.; Dong, X. Y.; Zang, S. Q. Robust multifunctional Zr-based metal-organic polyhedra for high proton conductivity and selective CO_2 capture. *J. Mater. Chem. A* **2018**, 6, 7724-7730.

(31) Liu, S. S.; Liu, Q. Q.; Huang, S. Z.; Zhang, C.; Dong, X. Y.; Zang, S. Q. Sulfonic and phosphonic porous solids as proton conductors. *Coord. Chem. Rev.* **2022**, 451, 214241.

(32) Sun, S. H.; Zhang, Q. C.; Ye, X. L.; Kashi, C. E.; Li, W. H.; Wang, G. E.; Xu, G. High-humidity sensor of a new trinuclear Ti_3-oxo cluster. *Chin. J. Struct. Chem.* **2022**, 41, 2203070-2203076.

(33) Li, S. J.; Zhao, Y.; Knoll, S.; Liu, R.; Li, G.; Peng, Q. P.; Qiu, P. T.; He, D. F.; Streb, C.; Chen, X. N. High proton-conductivity in covalently linked polyoxometalate-organoboronic acid-polymers. *Angew. Chem. Int. Ed.* **2021**, 60, 16953-16957.

(34) Sun, X. W.; Liu, S. M.; Zhang, S.; Dang, T. Y.; Tian, H. R.; Lu, Y.; Liu, S. X. High proton conductivity achieved by the self-assembly of POM-based acid-base adduct in SBA-15 over a wide range from -40 to 85 °C.

DOI: 10.14102/j.cnki.0254-5861.2022-0127

ACS Appl. Energy Mater. **2020**, 3, 1242-1248.
(35) Misra, A.; Kozma, K.; Streb, C.; Nyman, M. Beyond charge balance: counter-cations in polyoxometalate chemistry. *Angew. Chem. Int. Ed.* **2020**, 59, 596-612.
(36) Liu, Y. W.; Liu, S. M.; Lai, X. Y.; Miao, J.; He, D. F.; Li, N.; Luo, F.; Shi, Z.; Liu, S. X. Polyoxometalate-modified sponge-like graphene oxide monolith with high proton-conducting performance. *Adv. Funct. Mater.* **2015**, 25, 4480-4485.
(37) Buru, C. T.; Farha, O. K. Strategies for incorporating catalytically active polyoxometalates in metal-organic frameworks for organic transformations. *ACS Appl. Mater. Interfaces* **2020**, 12, 5345-5360.
(38) Ma, H. P.; Liu, B. L.; Li, B.; Zhang, L. M.; Li, Y. G.; Tan, H. Q.; Zang, H. Y.; Zhu, G. S. Cationic covalent organic frameworks: a simple platform of anionic exchange for porosity tuning and proton conduction. *J. Am. Chem. Soc.* **2016**, 138, 5897-5903.
(39) Gan, H. M.; Xu, N.; Qin, C.; Sun, C. Y.; Wang, X. L.; Su, Z. M. Equisize nesting of Platonic and Archimedean metal-organic polyhedra into a twin capsid. *Nat. Commun.* **2020**, 11, 4103.
(40) Li, X. X.; Zhao, D.; Zheng, S. T. Recent advances in POM-organic frameworks and POM-organic polyhedra. *Coord. Chem. Rev.* **2019**, 397, 220-240.
(41) Zhang, Y. T.; Gan, H. M.; Qin, C.; Wang, X. L.; Su, Z. M.; Zaworotko, M. J. Self-assembly of goldberg polyhedra from a concave $[WV_5O_{11}(RCO_2)_5(SO_4)]^{3-}$ building block with 5-fold symmetry. *J. Am. Chem. Soc.* **2018**, 140, 17365-17368.
(42) Zheng, S. T.; Zhang, J.; Li, X. X.; Fang, W. H.; Yang, G. Y. Cubic polyoxometalate-organic molecular cage. *J. Am. Chem. Soc.* **2010**, 132, 15102-15103.
(43) Chang, Q.; Meng, X. Y.; Ruan, W. J.; Feng, Y. Q.; Li, R.; Zhu, J. Y.; Ding, Y.; Lv, H. J.; Wang, W.; Chen, G. Y.; Fang, X. K. Metal-organic cages with $\{SiW_9Ni_4\}$ polyoxotungstate nodes. *Angew. Chem. Int. Ed.* **2022**, 134, e202117637.
(44) Gong, Y. R.; Qin, C.; Zhang, Y. T.; Sun, C. Y.; Pan, Q. H.; Wang, X. L.; Su, Z. M. Face-directed assembly of molecular cubes: in situ substitution of a predetermined concave cluster. *Angew. Chem. Int. Ed.* **2020**, 59, 22034-22038.
(45) Gong, Y. R.; Zhang, Y. T.; Qin, C.; Sun, C. Y.; Wang, X. L.; Su, Z. M. Bottom-up construction and reversible structural transformation of supramolecular isomers based on large truncated tetrahedra. *Angew. Chem. Int. Ed.* **2019**, 58, 780-784.
(46) Zhang, Z. J.; Wojtas, L.; Zaworotko, M. J. Organic-inorganic hybrid polyhedra that can serve as supermolecular building blocks. *Chem. Sci.* **2014**, 5, 927-931.
(47) Zhang, Y. T.; Wang, X. L.; Li, S. B.; Song, B. Q.; Shao, K. Z.; Su, Z. M. Ligand-directed assembly of polyoxovanadate-based metal-organic polyhedra. *Inorg. Chem.* **2016**, 55, 8770-8775.
(48) Liu, X.; Zhou, J.; Amarante, T. R.; Paz, F. A. A.; Fu, L. S. Vanadoborates: cluster-based architectures, preparation and properties. *Dalton Trans.* **2021**, 50, 1550-1568.
(49) Chen, H.; Yu, Z. B.; Bacsik, Z.; Zhao, H. S.; Yao, Q. X.; Sun, J. L. Construction of mesoporous frameworks with vanadoborate clusters. *Angew. Chem. Int. Ed.* **2014**, 53, 3608-3611.
(50) Wu, Y. L.; Li, X. X.; Qi, Y. J.; Yu, H.; Jin, L.; Zheng, S. T. $\{Nb_{288}O_{768}(OH)_{48}(CO_3)_{12}\}$: a macromolecular polyoxometalate with close to 300 niobium atoms. *Angew. Chem. Int. Ed.* **2018**, 57, 8572-8576.
(51) Jin, L.; Zhu, Z. K.; Wu, Y. L.; Qi, Y. J.; Li, X. X.; Zheng, S. T. Record high-nuclearity polyoxoniobates: discrete nanoclusters $\{Nb_{114}\}$, $\{Nb_{81}\}$, and $\{Nb_{52}\}$, and extended frameworks based on $\{Cu_3Nb_{78}\}$ and $\{Cu_4Nb_{78}\}$. *Angew. Chem. Int. Ed.* **2017**, 56, 16288-16292.
(52) Gong, Y. R.; Su, Z. M.; Wang, X. L. A polyoxometalate-based metal-organic polyhedron constructed from a $\{V_5O_9Cl\}$ building unit with rhombicub-octahedral geometry. *Acta Crystallogr. C Struct. Chem.* **2018**, 74, 1243-1247.
(53) Spek, A. L. PLATON SQUEEZE: a tool for the calculation of the disordered solvent contribution to the calculated structure factors. *Acta Crystallogr. C Struct. Chem.* **2015**, 71, 9-18.
(54) Liu, L.; Yin, L. Y.; Cheng, D. M.; Zhao, S.; Zang, H. Y.; Zhang, N.; Zhu, G. S. Surface-mediated construction of an ultrathin free-standing covalent organic framework membrane for efficient proton conduction. *Angew. Chem. Int. Ed.* **2021**, 60, 14875-14880.
(55) Lin, J. M.; Li, N.; Yang, S. P.; Jia, M. J.; Liu, J.; Li, X. M.; An, L.; Tian, Q. W.; Dong, L. Z.; Lan, Y. Q. Self-assembly of giant Mo_{240} hollow opening dodecahedra. *J. Am. Chem. Soc.* **2020**, 142, 13982-13988.
(56) Kang, D. W.; Kang, M. J.; Hong, C. S. Post-synthetic modification of porous materials: superprotonic conductivities and membrane applications in fuel cells. *J. Mater. Chem. A* **2020**, 8, 7474-7494.
(57) Lee, J.; Lim, D. W.; Dekura, S.; Kitagawa, H.; Choe, W. MOP x MOF: collaborative combination of metal-organic polyhedra and metal-organic framework for proton conductivity. *ACS Appl. Mater. Interfaces* **2019**, 11, 12639-12646.
(58) Chai, S. C.; Xu, F. R.; Zhang, R. C.; Wang, X. L.; Zhai, L.; Li, X.; Qian, H. J.; Wu, L. X.; Li, H. L. Hybrid liquid-crystalline electrolytes with high-temperature-stable channels for anhydrous proton conduction. *J. Am. Chem. Soc.* **2021**, 143, 21433-21442.
(59) Zhu, M. H.; Iwano, T.; Tan, M. J.; Akutsu, D.; Uchida, S.; Chen, G. Y.; Fang, X. K. Macrocyclic polyoxometalates: selective polyanion binding and ultrahigh proton conduction. *Angew. Chem. Int. Ed.* **2022**, 61, e202200666.
(60) Liu, W. J.; Dong, L. Z.; Li, R. H.; Chen, Y. J.; Sun, S. N.; Li, S. L.; Lan, Y. Q. Different protonic species affecting proton conductivity in hollow sphere-like polyoxometalates. *ACS Appl. Mater. Interfaces* **2019**, 11, 7030-7036.
(61) Zang, H. Y.; Chen, J. J.; Long, D. L.; Cronin, L.; Miras, H. N. Assembly of thiometalate-based $\{Mo_{16}\}$ and $\{Mo_{36}\}$ composite clusters combining $[Mo_2O_2S_2]^{2+}$ cations and selenite anions. *Adv. Mater.* **2013**, 25, 6245-6249.
(62) Zhang, F. M.; Dong, L. Z.; Qin, J. S.; Guan, W.; Liu, J.; Li, S. L.; Lu, M.; Lan, Y. Q.; Su, Z. M.; Zhou, H. C. Effect of imidazole arrangements on proton-conductivity in metal-organic frameworks. *J. Am. Chem. Soc.* **2017**, 139, 6183-6189.
(63) Shigematsu, A.; Yamada, T.; Kitagawa, H. Wide control of proton conductivity in porous coordination polymers. *J. Am. Chem. Soc.* **2011**, 133, 2034-2036.
(64) Lai, X. Y.; Liu, Y. W.; Yang, G. C.; Liu, S. M.; Shi, Z.; Lu, Y.; Luo, F.; Liu, S. X. Controllable proton-conducting pathways via situating polyoxometalates in targeting pores of a metal-organic framework. *J. Mater. Chem. A* **2017**, 5, 9611-9617.
(65) Liu, J. C.; Han, Q.; Chen, L. J.; Zhao, J. W.; Streb, C.; Song, Y. F. Aggregation of giant cerium-bismuth tungstate clusters into a 3D porous framework with high proton conductivity. *Angew. Chem. Int. Ed.* **2018**, 57, 8416-8420.

Received: May 18, 2022
Accepted: June 12, 2022
Published online: June 20, 2022
Published: July 25, 2022

DOI: 10.14102/j.cnki.0254-5861.2022-0127